Generation of fast protons in moderate-intensity laser–plasma interaction from rear sheath*

Tan Zhi-Xin(谭志新), Huang Yong-Sheng(黄永盛), Lan Xiao-Fei(兰小飞) ,
Lu Jian-Xin(路建新), Duan Xiao-Jiao(段晓礁), Wang Lei-Jian(王雷剑),
Yang Da-Wei(杨大为), Guo Shi-Lun(郭士伦), and Wang Nai-Yan(王乃彦)†

High Power Excimer Laser Laboratory, China Institute of Atomic Energy, Beijing 102413, *China*

(Received 1 June 2009; revised manuscript received 15 July 2009)

Forward fast protons are generated by the moderate-intensity laser–foil interaction. Protons with maximum energy 190 keV are measured by using magnetic spectrometer and CR-39 solid state track detectors along the direction normal to the rear surface. The experimental results are also modeled by the particle-in-cell method, investigating the time-varying electron temperature and the rear sheath field. The temporal and spatial structure of the sheath electrical field, revealed in the simulation, suggests that these protons are accelerated by target normal sheath acceleration (TNSA) mechanism.

Keywords: laser proton acceleration, target normal sheath acceleration
PACC: 5240K

1. Introduction

Over the last decade there has been a worldwide increasing interest in laser plasma acceleration due to the experimental demonstration of high accelerating gradient and ultra-low transversal emittance. Driven by the concept of compact tabletop accelerator for its potential applications such as hadron therapy,[1] proton imaging[2,3] and radioactive isotope generator,[4] laser plasma experiments have been switched from large scale laser systems to high repetition short pulse tabletop lasers.[5,6] In the present paper we report on experimental results about the protons generated by the interaction of moderate-intensity laser with aluminium targets. At this intensity there are two things that we can do. First, we measure proton emission by the interaction of moderate laser intensity with foil target, and the dependence of proton energy on the laser power density measured by our experiment extends the range of the scaling law to more low laser power density. Second, we identify the source of the protons since phenomena that only appear in relativistic intensity are eliminated, thereby conducing to profiling the acceleration mechanism in this regime.

Since the first forward collimated ion emission in laser–foil interaction[7,8] had reported, many experiments have been conducted all over the world, trying to figure out the underlying principle. The previous researches have shown that these protons came from the contamination layer on the target surface that existed persistently in vacuum system, independent of target materials.[9] But whether they come from the front side or rear side depends on many factors of the experimental setup. These protons may originate from the front side of the target, driven by the ponderomotive potential, and penetrate through the overdense plasma, or they come from the rear side accelerated by the rear sheath electrostatic field. Associated with the rear side acceleration is the target normal sheath acceleration (TNSA) model,[7] emphasizing the emissive direction and accelerating efficiency. Recent researches indicate that it is possible that both of these two mechanisms are effective simultaneously but the rear side acceleration accounts for the highest proton energy at optimum thickness.[10] A key parameter in the front side acceleration is the ponderomotive potential which induces a wakefield and envelopes the ions through the target. The ponderomotive potential is given by $\phi_{\rm p} = (\gamma - 1)m_{\rm e}c^2$, where $m_{\rm e}c^2$ is the electron rest energy, $\gamma = (1 + a_0^2)^{1/2}$, $a_0^2 = I\lambda^2/1.37 \times 10^{18}$. At relatively low energy intensity ($a_0 \ll 1$) these phenomena of ion enveloping even cannot happen. It is generally considered that in this regime the acceleration mechanism is mainly attributed to the rear side

*Project supported by the National Natural Science Foundation of China (Grant No. 10834008), and the State Key Development Program for Basic Research of China (Grant No. 2006CB806004).
†Corresponding author. E-mail: wangny@public.bta.net.cn
© 2010 Chinese Physical Society and IOP Publishing Ltd

acceleration. In our case the peak laser intensity is about 4×10^{16} W/cm^2, thus $\phi_{\rm p}\approx 4.1\times10^3$ V is pretty small compared with $\phi_{\rm p}=2.1\times10^5$ V at relativistic intensity ($a=1$). So we first assume that under this condition, if there is proton emission, the protons stem from the rear surface without penetrating through the target.

In 2001 Maksimchuk reported on 1.5 MeV proton generation at an intensity of 3×10^{18} W/cm^2 with 1.8 μm thin foil and the result was attributed to the consequence of the front side acceleration.[11] More detailed proton measurements on Mylar and metals were performed by Spencer *et al.*,[12] showing a maximum proton energy of 950 keV for 12 μm aluminium foil. At a higher laser intensity, over 10^{20} W/cm^2, a peak proton energy was reported to reach up to 17 MeV for a 5 μm thick aluminium foil,[13] implying the importance of hot electron recirculation. The influence of prepulse due to the amplified spontaneous emission (ASE) was investigated by Kaluza *et al.*[10] Accelerated protons from the rear and front sides were identified and at an optimum thickness the most energetic protons came from the rear side acceleration. At an intensity of $1.5\times10^{17}{\rm W}\cdot{\rm cm}^{-2}$ a proton spectrum serving as a check group was presented by Kishimura *et al.*[14] But for even low intensity there is no report and we show our measurements below.

2. Experimental measurement

The experiment was performed with a Ti:Sapphire chirped pulse amplification (CPA) laser system which delivered 10–30 mJ energy within 120 fs at 10 Hz. A p-polarized laser beam was incident obliquely at 45° with respect to the target normal, achieving a maximum focusing intensity of 4×10^{16} W/cm^2 on the target surface, averaging about 2×10^{16} W/cm^2 for our low energy concentration. The spectrum width of laser was about 10 nm around the central wavelength 744 nm and the contrast ratio was suppressed to below $10^{-5}:1$. Targets used in the experiments were 5 μm thin aluminium foils. The movement of the target was controlled by a step motor to ensure that each pulse hits a fresh surface. A magnetic spectrometer ($B=0.2$ T) and CR-39 track detectors were located along the direction normal to the rear surface. Ion emission was collimated by a 1-mm slit, passing through the magnetic spectrometer and hit the CR-39 solid state track detectors. The positions of tracks on the detectors after etching were used to calculate the corresponding kinetic energy of incident protons. Residual gas pressure in the vacuum chamber was measured to be around 2×10^{-3} Pa. The experimental arrangement is shown in Fig. 1.

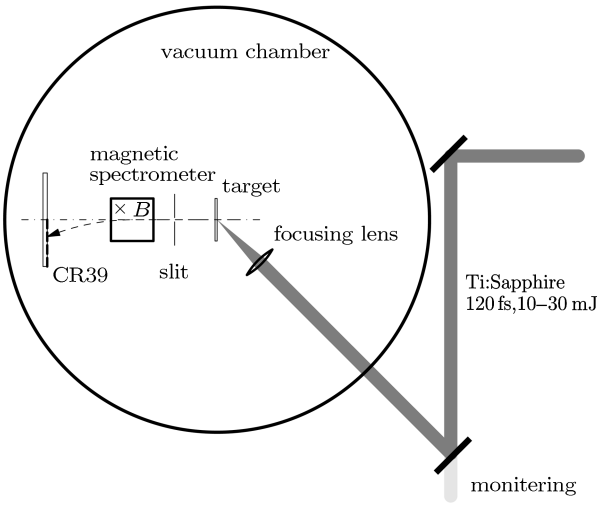


Fig. 1. Experimental setup for laser plasma interaction. The magnetic field is 0.2 T and emitted protons are collimated by a 1-mm slit. The maximum intensity of laser is about 4×10^{16} W/cm^2, and the laser is obliquely incident at 45°. The contrast ratio of prepulse is below 10^{-5}.

CR-39 solid state nuclear track detector is a plastic commonly used in nuclear physics and astrophysics for ion detection. One of the characteristics of solid state nuclear track detector is that this detector has a threshold which makes it insensitive to electrons and γ-rays because of insufficient energy deposition delivering to the detectors. This is a great advantage in complicated electromagnetic circumstances in laser–plasma experiments, but also a challenge to etching in working with the low energy ions. As mentioned in Ref. [15] the threshold of CR-39 plastic was about 100 keV . Due to the light mass the energy loss of proton is relatively small, and it will be slightly serious in the low energy case for fixing a track on the detectors with an appropriate etching manipulation. To address this problem we made an experiment in which CR-39 detectors were exposed to mono-energy proton produced by GIC4117 ion injector at Beijing Normal University. As shown in Fig. 2 the pits on CR-39 detectors are clear and uniform. This detector was irradiated by a 200 keV proton beam and etched in 6N NaOH solution at 70 °C for 6 h. It is suggested that the etching parameter is appropriate around this energy.

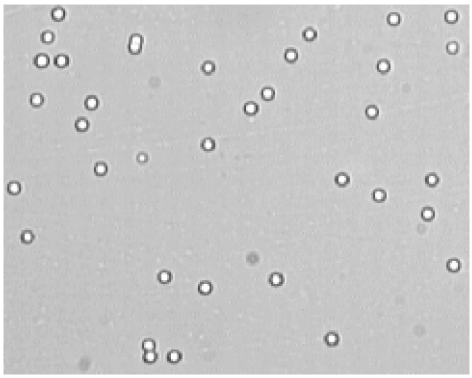


Fig. 2. Pits on CR-39 solid state track detector. This detector was exposed to 200 keV mono-energy protons and etched for 6 h in 6N NaOH solution at 70 °C.

Another important device is magnetic spectrometer, of which the field distribution is checked with Hall probes, showing the inhomogeneity inside is less than 2%. The accuracy of energy spectrum measurement is mostly dependent on slit width. The position of protons after passing through the magnetic spectrometer is calculated to be $y = [R - (R^2 - l^2)^{1/2}] + lL/(R^2 - l^2)^{1/2}$, where $R = mv/qB$ is the gyroradius, $l = 75$ mm is the length of magnetic field and $L = 130$ mm is the free space from the magnet to the CR-39 detectors.

The measurement result is shown in Fig. 3. We treat all tracks with deflections greater than 40 mm as proton tracks for a clear reason: if these were induced by other kinds of ions, such as C^{2+}, the ion energy should be lower than 60 keV which is below the CR-39 detector sensitive threshold and results in being wiped out through etching. An unexpected thing is that there are some tracks around the zero point.

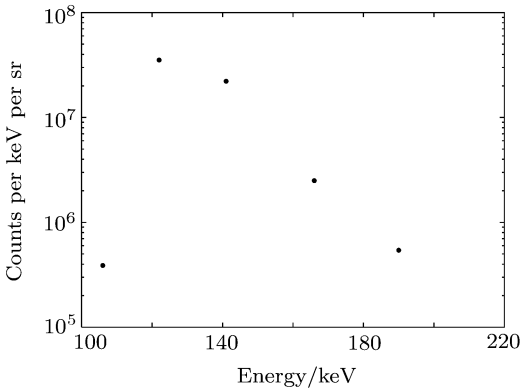


Fig. 3. Proton energy spectrum obtained from moderate-intensity laser irradiating 5 μm aluminium foil. Selective strips on CR-39 are collected and counted.

For a small and almost no deflection we cannot talk about their physical properties any more. The number density of protons is much lower than those given in other experimental reports. To accumulate enough data we use a magnetic spectrometer instead of a Thomson mass spectrometer and shot four thousand times. We attribute this low number density to our small overall energy delivered especially when our result is compared with the result in Ref. [14]. The half angle of emission cone is about $19° - 23°$, measured in a separate experiment with only CR-39 track detectors 20 mm away from the target back along the normal direction, showing no ring or uniform disk pattern.

As suggested, the collected maximum proton energies in short pulse laser plasma experiments are shown in Fig. 4. The targets used in the experiments were of copper or aluminium with a thickness of 5 μm. Our experimental result is marked as a lowest energy intensity of 4×10^{16} W/cm^2. A correlation between the maximum energy and $I\lambda^2$ is illustrated and the fitting result is $E_{\max} \sim (I\lambda^2)^{0.48}$. This fitting result is also consistant with the statement of Kishimura *et al.* in moderate intensity. The previous laser–plasma experiments and theories have established a strong relation between electron temperature I_e and $I\lambda^2$, which implies a direct relation between proton energy and electron temperature.[8] Therefore an investigation of the electron temperature and the electrical field structure, which directly accounts for the acceleration, should be helpful in understanding the accelerating process.

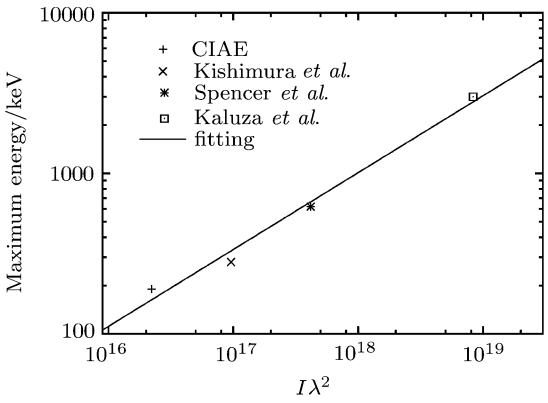


Fig. 4. Maximum proton energy as a function of $I\lambda^2$. Plus symbol represents our experimental result. Cross symbol denotes the data cited from Ref. [14] with using a 5 μm copper foil. Star symbol marks the data adopted from Ref. [12] with using a 6 μm aluminum foil. Square symbol represents the data cited from Kaluza.[10] All data are fitted to $E_{\max} \sim (I\lambda^2)^{0.48}$.

3. Simulation modeling

The experimental configuration was modeled with 1D particle-in-cell code which implements a Lorentz transformation to overcome the oblique incidence and

simplify the complexion of 2D PIC simulation.[16] The goal of our simulation is to check the electron temperature and the electrical field structure of the rear sheath. This transformation idea derives from Ref. [17] as illustrated in Fig. 5, where the laboratory frame is considered to move at a velocity of $v = c\sin\alpha$, where α is the incident angle of laser and c is the velocity of light in vacuum. Then all parameters are written in four-dimensional vector $\boldsymbol{x}^{\mu} = (x_1, x_2, x_3, x_4)^{\mathrm{T}}$ and transformed into the moving frame $x^{\mu}_{\mathrm{M}} = \boldsymbol{L}x^{\mu}_{\mathrm{L}}$, including those of the laser field and the plasma slice. A four-dimensional wave vector is transformed by matrix $\boldsymbol{L}$:

$$\begin{pmatrix} 1 & 0 & 0 & 0 \\ 0 & \Gamma & 0 & \mathrm{i}\beta\Gamma \\ 0 & 0 & 1 & 0 \\ 0 & -\mathrm{i}\beta\Gamma & 0 & \Gamma \end{pmatrix} \begin{pmatrix} k\cos\alpha \\ k\sin\alpha \\ 0 \\ \dfrac{\mathrm{i}}{c}\omega \end{pmatrix} = \begin{pmatrix} k\cos\alpha \\ 0 \\ 0 \\ \dfrac{\mathrm{i}}{c}\omega\cos\alpha \end{pmatrix}, \tag{1}$$

where $\beta = \sin\alpha$, $\Gamma = 1/\cos\alpha$. Obviously there is only x component of wave vector in the moving frame. Thus the Poynting vector is normally incident on the plasma slice, and common 1D leap-frog algorithm can be applied. All diagnostics is carried out in the laboratory frame after an inverse Lorentz transformation. We modifier the velocity diagnostics to output the kinetic energy of each particle, then make a histogram to calculate the electron temperature.

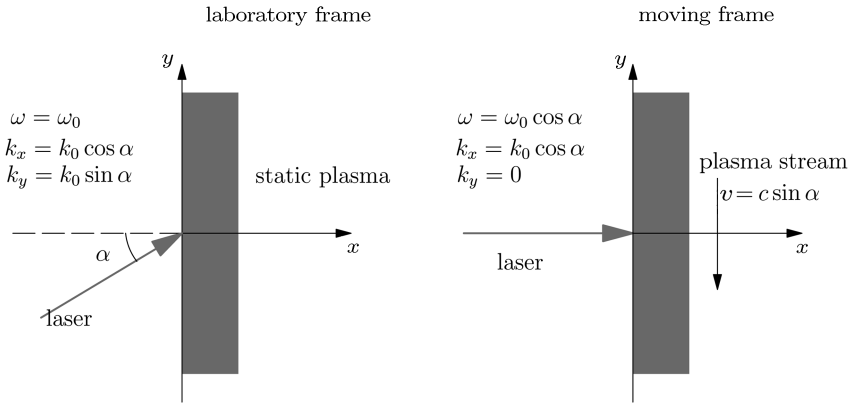


Fig. 5. Lorentz transformation scheme. The left is the configuration in laboratory frame. Laser beam is incident at angle α. The moving frame is drawn as the right one at a velocity $v_y = c\sin\alpha$ relative to the laboratory frame. Four-dimensional wave vector after the Lorentz transformation is normally incident on the plasma slice.

The simulation length is about 26.4 μm. Ideal p-polarized laser pulse is incident from the left at an angle of 45° with respect to the plasma surface. The dimensionless amplitude is set to be 0.15. Laser input starts at time $t = 0$ with a pulse length of 55 periods. The plasma slice is 5 μm thick, composed of electrons and Al^{3+} macro-particles at weight ratio 1:50000. The ion density is $35n_{\mathrm{c}}$, about 1.5×10^{21} cm^{-3}. An important idea in our simulation is that we choose the electron temperature as an index for our simultaion when the simulation parameters are considered, which was experimentally measured to be 18 keV from the frontside of the target in the same condition.

4. Results and discussion

As shown in Fig. 6 (left), in our simulation the electron temperature is about 10 keV and 16.2 keV at time $\omega_0 t = 20$ and 72 respectively. These electron spectra are of almost quasi-equilibrium which should be the results of a small electromagnetic beam input ($a = 0.15$). The electron temperature as a time-varying function is illustrated in the right. The heating progress starts at about $\omega_0 t = 10$. The electron temperature grows rapidly and reaches a maximum value at about $\omega_0 t = 80$, then slowly drops down. This evolution of the temperature

shows that the plasma is approximately isothermal in a time range from $\omega_0 t = 50$ to $\omega_0 t = 110$, which seems the support for the theoretical expansion model.[18,19] A similar consideration was also reported in Ref. [20], but showed the discrepancy with the theoretical model in the case of high intensity.

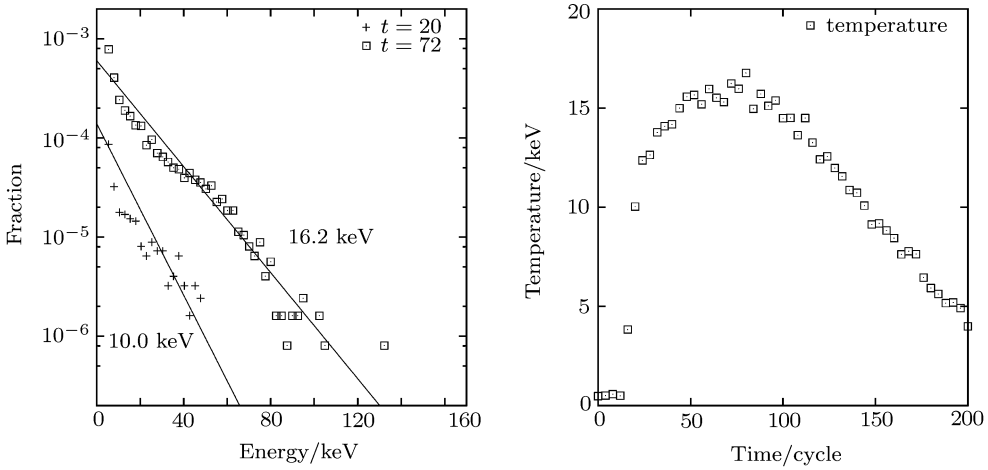


Fig. 6. Electron temperature evolution given by PIC simulation. On the left side is the electron energy spectrum at time $\omega_0 t = 20$ and 72, separately. Electron temperature as a function of time is drawn on the right side. The electrons are shown to be heated up to 17 keV and then slowly cool down.

The sheath electrical field along the x-axis in laboratory frame is plotted as a function of time in Fig. 7 (left). It is shown that the rear sheath electrical field is built at about $\omega_0 t = 40$, and it reaches a maximum value at time $\omega_0 t = 64$, then rapidly falls down. The duration of sheath field is about $80 - 35 = 45$ periods, just as the duration of the laser pulse. This time structure is inconsistent with that of plasma temperature evolution which shows an FWHM(full width at half maximum) greater than $2\tau_{\rm L}$. This value is also shorter than $\tau_{\rm acc} = 1.3\tau_{\rm L}$ given by the plasma expansion model in Ref. [20]. It is considered that under low intensity the sheath is more fragile and collapse quickly while the electron temperature of thick target falls down gradually. The average electrical field intensity for acceleration is

$$\overline{E} = \frac{\sqrt{2}}{2} E_{\max} = 1.8 \times 10^{11} \text{ V/m}, \qquad (2)$$

where $E_{\max} = 0.4E_0$, $E_0 = m\omega_0 c/e = 6.4 \times 10^{11}$ V/m. An important parameter in the TNSA model is the Debye length which is also illustrated in our simulation, see Fig. 7 (right). The FWHM of the sheath length is calculated to be about $(21.415 - 21.298) \times 0.800 = 0.09$ μm, where 0.8 μm is the laser wavelength. If we take the electron temperature to be between $\omega_0 t = 50$ and $\omega_0 t = 100$ as an isothermal progress at 15 keV, then in our case this electrical amplitude estimated in the TNSA model leads to

$$E_{\rm TNSA} = \frac{kT_{\rm e}}{e\lambda_{\rm D}} \approx 1.67 \times 10^{11} \text{V/m}, \qquad (3)$$

only a bit lower than the average accelration field $\overline{E} = 1.8 \times 10^{11}$ V/m. The maximum accelerating gradient is up to 2.6×10^{11} V/m, corresponding to $a = 0.4$, and the delta function like electrical field is four times as strong as the initial input $E_x/E_0 = 0.1$. This sheath field structure is in accordance with the description of TNSA model, consistent with our presumption that rear sheath acceleration is effective at moderate intensity. Furthermore, for a proton passing through a 5 μm thick aluminium target, the energy is calculated to be at least 450 keV in SRIM.[1)] But from the scale law in Fig. 4, it is impossible to generate such highly energetic protons in our experimental condition and these fast protons in our measurements should originate from the rear sheath. Therefore, with a moderate laser intensity, although the input energy intensity is not powerful enough to create a strong wakefield, the hot electrons accumulated around the rear surface are still capable of setting up a strong sheath field which accounts for the fast proton acceleration.

[1)] http://www.srim.org

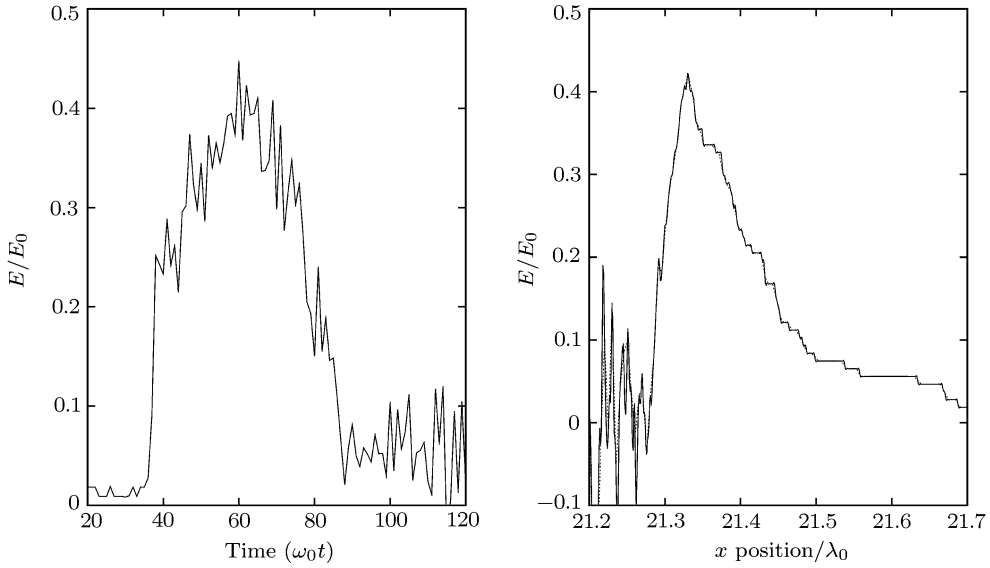


Fig. 7. Time-varying sheath field at position $x = 21.325\lambda_0$ (left) and the spatial distribution of the rear sheath electrical field at time $\omega_0 t = 64$ (right). The coordinate of the target rear surface is $21.25\lambda_0$.

5. Conclusion

We observe fast protons emitted in moderate-intensity laser–foil interactions along the direction normal to the target rear surface at a maximum proton energy of about 190 keV. The experiment is modeled by the particle-in-cell method to obtain a detailed investigation. Simulation reconstruction of rear sheath electrical field suggests that protons originate from the rear surface and they are accelerated by the sheath electrical field.

Acknowledgement

The authors wish to make a grateful acknowledgement for the assistance of the short-pulse laser group and Professor Wang Guang-Pu of Beijing Normal University.

References

[1] Bulanov S and Khoroshkov V S 2002 *Plasma Physics Reports* **28** 453

[2] Borghesi M, Campbell D H, Schiavi A, Haines M G, Willi O, MacKinnon A J, Patel P, Gizzi L A, Galimberti M, Clarke R J, Pegoraro F, Ruhl H and Bulanov S 2002 *Phys. Plasmas* **9** 2214

[3] Teng J, Hong W, Zhao Z Q, Wu S C, Qin X Z, He Y L, Gu Y Q and Ding Y K 2009 *Acta Phys. Sin.* **58** 1635 (in Chinese)

[4] Fritzler S, Malka V, Grillon G, Rousseau J P, Lefebvre F, Burgy E, McKenna P, d'Humières E and Ledingham K W D 2003 *Appl. Phys. Lett.* **83** 3039

[5] Fang Z B, Shen B F, Cheng C F and Zhang X M 2005 *Chin. Phys.* **14** 1850

[6] He M Q, Dong Q L, Shen Z M, Weng S M, Chen M, Wu H C and Zhang J 2009 *Acta Phys. Sin.* **58** 363 (in Chinese)

[7] Hatchett S P, Brown C G, Cowan T E, Henry E A, Johnson J S, Key M H, Koch J A, Langdon A B, Lasinski B F, Lee R W, Mackinnon A J, Pennington D M, Perry M D, Phillips T W, Roth M, Sangster T C, Singh M S, Snavely R A, Stoyer M A, Wilks S C and Yasuike K 2000 *Phys. Plasmas* **7** 2076

[8] Wilks S C, Langdon A B, Cowan T E, Roth M, Singh M, Hatchett S, Key M H, Pennington D, MacKinnon A and Snavely R A 2001 *Phys. Plasmas* **8** 542

[9] Gitomer S J, Jones R D, Begay F, Ehler A W, Kephart J F and Kristal R 1986 *Physics Fluids* **29** 2679

[10] Kaluza M, Schreiber J, Santala M I K, Tsakiris G D, Eidmann K, Meyer-ter Vehn J and Witte K J 2004 *Phys. Rev. Lett.* **93** 045003

[11] Maksimchuk A, Gu S, Flippo K, Umstadter D and Bychenkov V Yu 2000 *Phys. Rev. Lett.* **84** 4108

[12] Spencer I, Ledingham K W D, McKenna P, McCanny T, Singhal R P, Foster P S, Neely D, Langley A J, Divall E J,

Hooker C J, Clarke R J, Norreys P A, Clark E L, Krushelnick K and Davies J R 2003 *Phys. Rev.* E **67** 046402

[13] Mackinnon A J, Sentoku Y, Patel P K, Price D W, Hatchett S, Key M H Andersen C, Snavely R and Freeman R R 2002 *Phys. Rev. Lett.* **88** 215006

[14] Kishimura H, Morishita H, Okano Y H, Okano Y, Hironaka Y, Kondo K, Nakamura K G, Oishi Y and Nemoto K 2004 *Appl. Phys. Lett.* **85** 2736

[15] Beg F N, Bell A R, Dangor A E, Danson C N, Fews A P, Glinsky M E, Hammel B A, Lee P, Norreys P A and Tatarakis M 1997 *Phys. Plasmas* **4** 447

[16] Licheters R, Pfund R E W and Meyer–ter–Vehn J 2000 *LPIC^{++} A Parrellel One-dimensional Relativistic Electromagnetic Paticle-In-Cell Code for Simulating Laser-Plasma-Interaction*

[17] Bourdier A 1983 *Phys. Fluids* **26** 1804

[18] Mora P 2005 *Phys. Rev.* E **72** 056401

[19] Huang Y S, Bi Y J, Duan X J, Lan X F, Wang N Y, Tang X Z and He Y X 2008 *Appl. Phys. Lett.* **92** 031501

[20] Fuchs J, Antici P, D'Humières E, Lefebvre E, Borghesi M, Brambrink E, Cecchetti C A, Kaluza M, Malka V, Manclossi M, Meyroneinc S, Mora P, Schreiber J, Toncian T, Pepin H and Audebert P 2006 *Nature Physics* **2** 48